Characterization of Aggregate Structure in Mercerized Cellulose/LiCl·DMAc Solution Using Light Scattering and Rheological Measurements

Hajime Aono, Daisuke Tatsumi,* and Takayoshi Matsumoto

Division of Forest and Biomaterials Science, Graduate School of Agriculture, Kyoto University, Kyoto 606-8502, Japan

Received November 22, 2005; Revised Manuscript Received February 10, 2006

The structure of a semidilute solution of mercerized cellulose (CC1m) in 8% (w/w) LiCl·DMAc, which contained some aggregates, was investigated using static and dynamic light scattering measurements. The static scattering function of the polymer solution containing a small amount of aggregates can be separated into fast- and slow-mode components by combining static and dynamic light scattering measurements. The osmotic modulus was identical for the fast-mode component of the CC1m solutions and the native cellulose (CC1) solutions, in which cellulose is dispersed molecularly. This indicates that the molecularly dispersed component of the CC1m solutions has an identical conformation with the cellulose molecules in the CC1 solutions. The correlation length was also identical for the fast-mode components of CC1m solutions and the CC1 solutions, indicating that these solutions have the same mesh size of the polymer entanglement. These observations for the fast-mode components are consistent with the concentration dependence of the zero shear rate viscosity and the plateau modulus estimated in the rheological measurements. The slow-mode component, on the other hand, gave information on the aggregate structure in the CC1m solution. The radius of gyration of the aggregate structure estimated from the slow-mode component was about 70 nm, which is independent of the concentration of the solution. The plots for particle scattering factor of the slow-mode component lay between the theoretical curve of a sphere and a Gaussian chain, implying that the structure of the aggregate in the CC1m solution is like a multiarm polymer. A characteristic time of the slow-mode component calculated with the translational diffusion coefficient and the radius of gyration were almost identical with the relaxation time of the long-time relaxation observed in the rheological measurements. This indicates that the long-time relaxation of CC1m solutions originates in the translational diffusion of the aggregate structure in the solution.

Introduction

Light scattering measurements are very sensitive to some large structures in the solutions, so that aggregate structures formed in the solution sometimes make the characterization of the polymer solution difficult. For example, the enhanced low-angle scattering of polystyrene semidilute solutions, which cannot be explained by the theories available at present, were reported.[1−4] These anomalous low-angle scattering results were thought to be derived from the aggregate structures in the solution. For some polysaccharide solutions which form aggregates with increasing polymer concentration, the "true molecular mass at the concentration" was estimated from the osmotic modulus ratio of a master curve, which was derived from the data in the nonaggregating concentration region, to the measured value in the aggregating concentration region using SLS measurements.[5,6] However, this method assumes the same fractal dimension of the polymer molecule and the aggregate structure. Moreover, the estimated value is the weight average of the molecularly dispersed component and the aggregated component. Thus, this method is not suitable for the characterization of the each component separately especially the molecularly dispersed component.

In colloid science, it is one of the most important themes of fundamental researches to determine the form and the dimension of the aggregates. Dynamic light scattering (DLS) measurement is one of the most common methods for the analysis of the solution containing aggregate structures. It is very convenient for qualitative analysis such as the confirmation of the existence of aggregate structures but is not for the quantitative analysis. For example, an accurate hydrodynamic radius may not be estimated using the viscosity of the solvent and the diffusion coefficient evaluated from the DLS measurement, because of the interference in the diffusion of the aggregate structures by the surrounding dispersed polymers.

Recently, on the basis of the dynamic mean field theory, Kanao et al.[7] suggested a new method to separate a static scattering function into two components of different mobility by combining SLS measurements with DLS measurements. This method makes it possible for the scattering function of the molecularly dispersed component and the one of the aggregate structure to be analyzed independently. Such a separation had been performed[8] before Kanao et al.; however, the physical meanings had not been clarified theoretically then.

We have reported the differences in the solubility and the rheological properties of the cellulose solutions derived from different biological sources (plants, bacteria, and ascidians) in 8% (w/w) LiCl·DMAc or 8% (w/w) LiCl/1,3-dimethy-2-limidazolidinone (DMI).[9−11] In particular, the differences in the concentration-dependence of the zero shear rate viscosity indicate that these celluloses take different conformations in 8% (w/w) LiCl·DMAc. Moreover, we have investigated the effect of mercerization,[12] immersing solid cellulose in an alkaline

* To whom correspondence should be addressed. Phone: +81-75-753-6249. Fax: +81-75-753-6300. E-mail: daiske9@kais.kyoto-u.ac.jp.

10.1021/bm050889h CCC: $33.50
Published on Web 03/18/2006

solution such as NaOHaq, on the cellulose solution in terms of rheological and dilute solution properties in 8% (w/w) LiCl·DMAc.[13] From the viscoelastic measurements of the semidilute solutions, a long time relaxation was found only for the mercerized cellulose solution; this indicates that some heterogeneous structures such as aggregates were formed in the mercerized cellulose solution. These celluloses with different solution properties should have different molecular properties and structures in the solution; however, the details are still unclear. For the wider applications of these celluloses, it would be useful to clarify the structures and properties in solutions.

In our previous paper,[14] we investigated the structural analysis of cotton cellulose (CC1), which is the most common cellulose derived from higher plants, in semidilute solution in 8% (w/w) LiCl·DMAc by static light scattering (SLS) measurements. The data from SLS measurements are excellently related with those from the rheological measurements[9,10] by the scaling relationships, and the conformation of the cellulose molecule in CC1 solutions was discussed. Mercerized cellulose solutions, however, contain some aggregate structures, and this method cannot be applied because the scattering function of the solution contains a contribution from the component of molecularly dispersed molecules and the one from the aggregate structure.

In this study, the structural analysis of a mercerized cellulose semidilute solution in 8% (w/w) LiCl·DMAc was done using SLS and DLS measurements. The static scattering functions estimated from SLS measurements were separated into the contribution of the molecularly dispersed component (fast-mode component) and one of the aggregate structures (slow-mode component) using the method suggested by Kanao et al.[7]

Materials and Methods

Materials and Preparation of Solutions. Cotton cellulose (CC1) was used as a native cellulose sample. The characteristics of CC1 obtained from the light scattering measurements are as follows:[14] $M_w = 82.5 \times 10^4$, $A_2 = 8.55 \times 10^{-4}$ g^{-2}·mL·mol, $R_g = 61.3$ nm; where M_w, A_2, and R_g represent the weight average molecular weight, the second virial coefficient, and the *z*-average mean square radius of gyration.

Mercerized cellulose sample (CC1m) was prepared from the CC1 using the following procedure:[13] the CC1 was soaked in 17.5% (w/w) sodium hydroxide solutions (bath ratio: 1 g of cellulose/100 g of NaOHaq) at room temperature for 1 h. NaOHaq was subsequently removed by filtering through 1G2 glass filter, and the swollen cellulose samples were washed in 10% (w/w) acetic acid followed by enough washing with distilled water until the electric conductivity of the washing water becomes is equal to that for distilled water. Water was then removed by soaking in methanol and filtering through a Büchner funnel.

The dissolution of cellulose in LiCl·DMAc requires a pretreatment of cellulose.[15−17] In this study, the solvent exchange method consisting of the sequential soaking cellulose in water, acetone, and DMAc was employed. The procedure was performed as described in the previous paper.[9,10] To obtain a completely dissolved state, the solutions prepared were allowed to stand at room temperature for 2∼3 months before the measurements.

Measurements. Static light scattering (SLS) measurements were performed with a light scattering photometer SLS-5000HM (Otsuka Electronics Co., Ltd.) under the following conditions: wavelength, $\lambda_0 = 632.8$ nm (He−Ne laser); scattering angles, $30° \le \theta \le 150°$; temperature, 25 °C. The sample solutions were filtered by PTFE membrane filters (Toyo Roshi Kaisha Ltd.) with pore sizes of 0.2 or 0.45 μm, sealed up, and allowed to stand overnight before the measurements. The value of the specific refractive index increment, $\partial n/\partial c$, used was 0.0575 mL/g, which is given by McCormick et al.[16]

Dynamic light scattering (DLS) measurements were performed with the same light scattering photometer as SLS measurements equipped with an ALV-5000/E correlator (ALV Co.) at 25 °C. The distribution of the decay rate, $G(\Gamma_i)$, was estimated by the regularized fitting with the CONTIN method[18,19] from $g^{(2)}(q, \tau)$ obtained by DLS measurements.

Dynamic viscoelasticity measurements were performed with a cone-plate type rheometer Rheosol-G2000 (UBM Co., Ltd.). Radii of the cone and plate were 50 mm, and the angle of the cone was 2°. The rheometer was equipped with a reservoir to prevent sample drying during the measurements. The dynamic viscoelasticity measurements were performed at various temperatures ranging from −15 to +80 °C. All of the data were reduced to the data at a reference temperature of 30 °C by the time−temperature superposition principle.[20]

Analysis of the Data from SLS Measurements. The results of SLS measurements were analyzed using the apparent molecular mass, $M_{app}(c)$, and the apparent radius of gyration, $R_{g,app}(c)$, defined as follows:

$$\frac{Kc}{R_{\theta\to 0}(c)} = \frac{1}{RT}\left(\frac{\partial \Pi}{\partial c}\right) \equiv \frac{1}{M_{app}(c)} \tag{1}$$

$$\frac{Kc}{R_\theta(c)} = \frac{1}{M_{app}(c)}\left(1 + \frac{1}{3}R_{g,app}{}^2(c)q^2 - \cdots\right) \tag{2}$$

where K, $R_\theta(c)$, R, T, Π, and q represent the optical constant, the excess Rayleigh ratio of the solution at a scattering angle (θ), the concentration (c), the gas constant, the absolute temperature, the osmotic pressure, and the magnitude of the scattering vector. As shown in eq 1, $M_{app}(c)$ is a quantity proportional to the osmotic modulus, ($\partial c/\partial \Pi$). $R_{g,app}(c)$ indicates the *z*-average mean square radius of gyration at $c \to 0$ and the mesh size of polymer entanglement in the semidilute region.[21] $R_{g,app}(c)$ is equivalent to the correlation length, ξ, given by the Ornstein−Zernike equation ($I(q) = I(0)/(1+\xi^2q^2)$) and they are related in the following equation:

$$R_{g,app}(c) = \sqrt{3}\xi$$

Separation of $R_\theta(c)/Kc$ Combining SLS and DLS Measurement. On the basis of the dynamic mean field theory, Kanao et al. showed the following:[7] when a bimodal distribution is observed by DLS measurements for the polymer solution containing a small amount of aggregates, the monomer-unit static structure factor, $\hat{S}_m(q)$ ($= R_\theta(c)/KcM_0$, where M_0 is the molecular weight of the monomer unit), estimated from SLS measurements can be separated into two components with different mobilities as

$$\hat{S}_{fast}(q) = \hat{S}_m(q) \sum_{i\in fast} A(\Gamma_i) \tag{3}$$

$$\hat{S}_{slow}(q) = \hat{S}_m(q) \sum_{i\in slow} A(\Gamma_i) \tag{4}$$

where $\hat{S}_m(q)_{fast}$ and $\hat{S}_m(q)_{slow}$, represent the fast- and slow-mode components of the static structure factor. $A(\Gamma_i)$ is the normalized $G(\Gamma_i)$ as follows: $\sum_i^n A(\Gamma_i) = 1$ (i.e., $A(\Gamma_i) = G(\Gamma_i)/\sum_{i=1}^n G(\Gamma_i)$). $R_\theta(c)/Kc$ ($= M_0\hat{S}_m(q)$) can be separated like $\hat{S}_m(q)$ as follows because M_0 is constant:

$$(R_\theta(c)/Kc)_{fast} = (R_\theta(c)/Kc) \sum_{i\in fast} A(\Gamma_i) \tag{5}$$

$$(R_\theta(c)/Kc)_{slow} = (R_\theta(c)/Kc) \sum_{i\in slow} A(\Gamma_i) \tag{6}$$

As reported in our previous paper,[13] the CC1m solution in 8% (w/w)

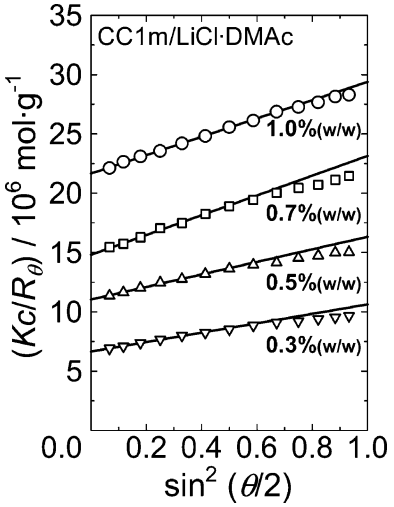

Figure 1. Zimm plot for the CC1m solution in 8% (w/w) LiCl·DMAc. K, c, and R_θ represent the optical constant, the concentration of the polymer, and the excess Rayleigh ratio at scattering angle, θ.

LiCl·DMAc showed the bimodal distribution of $G(\Gamma_i)$ in the semidilute region. In this study, eqs 5 and 6 were applied to the CC1m solutions to separate the scattering function into the fast- and slow-mode components, and each component was analyzed, respectively.

Results

SLS Measurements. The Zimm plots, $Kc/R_\theta(c)$ obtained from SLS measurements plotted versus sin^2 (θ/2), for CC1m solutions are shown in Figure 1. The concentration, c, ranged from 3.05 to 10.0 mg/mL (corresponding to 0.3∼1.0% (w/w)). The slope of the plots became larger with increasing concentration of the solution, and the plots at higher angles deviated from the straight lines that are fitted for lower angles (solid line). This observation is different from that obtained from CC1 solutions,[14] in which both liner and parallel sin^2(θ/2) dependence were observed up to the highest concentration examined (≈1.3% (w/w)). This indicates that the aggregate structure, which is larger than the molecularly dispersed cellulose, was formed in CC1m solutions.

DLS Measurements. Figure 2 shows $G(\Gamma_i)$ for the CC1m semidilute solutions (c_w = 0.3∼1.0% (w/w)) obtained from DLS measurements at θ = 30°. The apparent hydrodynamic radius, R_H, calculated with the Einstein−Stokes relation represented by eq 7 is also shown in the top axis in Figure 2

$$R_H = \frac{k_B T}{6\pi\eta_s D_T} \tag{7}$$

where k_B, T, η_s, and D_T represent Boltzmann constant, absolute temperature, viscosity of the solvent, and the translational diffusion coefficient. D_T was calculated as $D_T = \Gamma_i/q^2$, and in Figure 2, $G(\Gamma_i)$ was normalized at the maximum and sifted vertically. The bimodal distribution of $G(\Gamma_i)$ was observed for all of the samples corresponding to our previous study.[13] The peak of the higher decay rate (fast-mode) in $G(\Gamma_i)$ tended to shift to larger Γ_i (i.e., smaller R_H) with an increase in the polymer concentration. In contrast, the peak of slower decay rate (slow-mode) tended to shift to smaller Γ_i, (i.e., larger R_H) with an increase in the polymer concentration. The data in Figure 2 shows a minute relaxation between fast and slow mode. However, these peaks were very small and showed low reproducibility especially at higher angles. Then, these peaks were ignored in the analysis in this study.

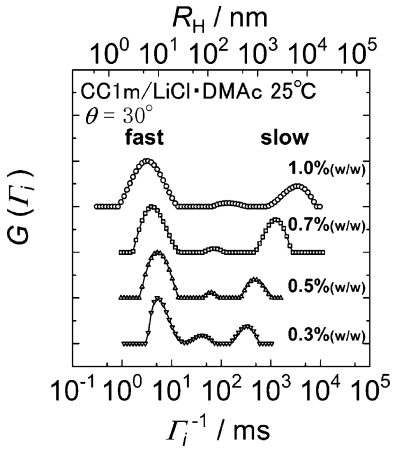

Figure 2. Decay late distributions, $G(\Gamma_i)$, plotted versus the reciprocal of decay rate, Γ_i^{-1}, for CC1m solutions in 8% (w/w) LiCl·DMAc. $G(\Gamma_i)$ for each concentration was normalized at the maximum and sifted vertically, and each scale unit on the y axis represents 1. Apparent hydrodynamic radius, R_H, calculated with the Einstein−Stokes relation $D_T = k_B T/6\pi\eta_s R_H$ is shown in the top axis. Here k_B, T, and η_s are Boltzmann constant, the absolute temperature, and the viscosity of the solvent. D_T is the translational diffusion coefficient calculated with $D_T = \Gamma_i/q^2$.

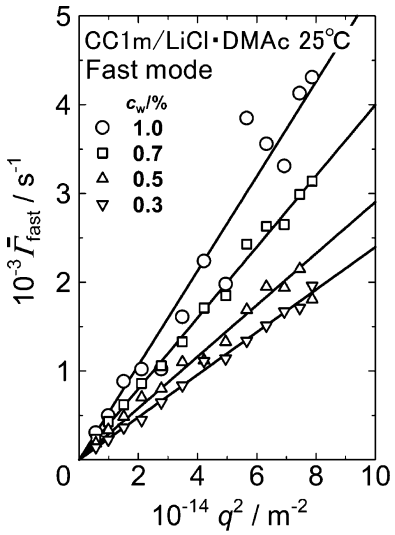

Figure 3. Mean decay rates for the fast-mode, $\bar{\Gamma}_{fast}$, plotted versus the square of the magnitude of scattering vector, q^2.

The mean decay rate of a peak in $G(\Gamma_i)$, $\bar{\Gamma}$, was obtained by the following equation:

$$\ln \bar{\Gamma} = \frac{\sum_i G(\Gamma_i) \ln \Gamma_i}{\sum_i G(\Gamma_i)} \tag{8}$$

Figures 3 and 4 show the q^2 dependence of $\bar{\Gamma}$ for the fast- and slow-mode calculated with eq 8. In both the fast- and slow-modes, $\bar{\Gamma}$ was proportional to q^2 within the measured q range, though some data points varied. The slopes in Figures 3 and 4 give the cooperative diffusion coefficient for the fast-mode components, $\bar{D}_{T,fast}(c)$, and the mean translational diffusion coefficient for the slow-mode components, $\bar{D}_{T,slow}(c)$, respectively. The apparent hydrodynamic radii, $\bar{R}_{H,fast}(c)$ and $\bar{R}_{H,slow}(c)$, were calculated by $\bar{D}_{T,fast}(c)$ and $\bar{D}_{T,slow}(c)$ using eq 7. The diffusion coefficient and the apparent hydrodynamic radius for each mode obtained by the DLS measurements are shown in Table 1.

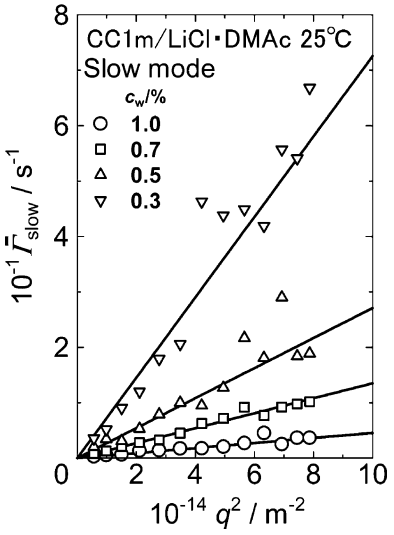

Figure 4. Mean decay rates for the slow-mode, $\bar{\Gamma}_{slow}$, plotted versus the square of the magnitude of scattering vector, q^2.

Discussion

Fast-Mode Component. Figure 5 shows the $\sin^2(\theta/2)$ dependence of $Kc/R_\theta(c)_{fast}$ for CC1m solutions obtained from the results of the DLS and the SLS measurements using eq 5. When a slight peak was observed between the fast- and slow-mode, the peak was ignored, and $A(\Gamma_i)$ was renormalized as $\sum_{i\in fast} A(\Gamma_i) + \sum_{i\in slow} A(\Gamma_i) = 1$.[7]

The dependence of $Kc/R_\theta(c)_{fast}$ on $\sin^2(\theta/2)$ for CC1m solutions was almost liner and parallel, which was similar to the results for CC1 solutions.[14]

Figure 6 shows the concentration dependence of $M_{app}(c)$ ($= (\partial\Pi/\partial c)/RT$) for CC1m solutions and their fast-mode component estimated from the extrapolated straight line in Figures 1 and 5 using eq 1. The data obtained from the CC1 solution are also plotted in Figure 6. The value of $1/M_{app}(c)$ for CC1m was a little smaller than that of CC1 for all of the concentration region examined. This should be the effect of the aggregate structure in CC1m solutions. However, $1/M_{app}(c)$ for the fast-mode component of CC1m solutions was almost identical with the data from CC1 solutions, and they were proportional to $c^{1.16}$. This indicates that the molecularly dispersed component in the CC1m solution takes the same conformation as CC1 molecules in 8% (w/w) LiCl·DMAc. This is consistent with the same concentration dependence of zero shear rate viscosity for CC1 and CC1m solutions.[13] In our previous paper,[14] the exponent of 1.16 gave the relationship between the radius of gyration and molecular weight as $R_g \propto M^{0.62}$ using the scaling relationship ($m = 1/(3\nu - 1)$) derived by de Gennes.[21]

Figure 7 shows the concentration dependence of $R_{g,app}(c)$ for CC1m solutions and their fast-mode component estimated from the extrapolated straight line in Figures 1 and 5 using eq 2. The data obtained from the CC1 solution are also plotted in Figure 7. For all of the concentration regions examined, the value of $R_{g,app}(c)$ for CC1m was larger than that of CC1. This could be caused by the aggregate structure, which is larger than the mesh size of polymer entanglement, in CC1m solutions. On the other hand, $R_{g,app}(c)$ for the fast-mode component of CC1m solutions was almost identical with the data from CC1 solutions. This indicates that the mesh size of polymer entanglements is almost identical for CC1m and CC1 solutions. This is supported by the result of the rheological measurements where the plateau modulus of CC1m solutions was identical with that of the CC1 solutions.[13]

Slow-Mode Component. $(R_\theta(c)/Kc)_{slow}$ obtained from the separation of $R_\theta(c)/Kc$ using eq 6 should represent the scattering function of the aggregate structures in the CC1m solution. The Guinier equation is more suitable for the estimation of the size of aggregate structure than the Ornstein−Zernike equation (eq 2), which is suitable for the estimation of the characteristic length of "cavity structure" such as the size of coils or mesh:

$$\ln(R_\theta(c)/Kc)_{slow} = \ln M_{app,slow} - \frac{1}{3}R_{g,slow}q^2 + \cdots \quad (9)$$

Figure 8 shows the Guinier plot, plotting $\ln(R_\theta(c)/Kc)$ versus q^2, for the slow-mode component of CC1m solutions. In Figure 8, the plots were shifted vertically by a factor, X, to avoid the overlapping of the plots. The mean square radius of gyration for the aggregate structures in the CC1m solution, $R_{g,slow}(c)$, was estimated from the extrapolated straight line in Figure 8 using eq 9 (Table 1). The value of $R_{g,slow}(c)$ was almost constant ($R_{g,slow}(c) \approx 70$ nm), though the value of $\bar{R}_{H,slow}(c)$ estimated from the DLS measurements was increased remarkably with increasing polymer concentration. This implies that the correct $\bar{R}_{H,slow}(c)$ is not evaluated by eq 7 using the viscosity of the solvent, η_s, because of the interference in the diffusion of the aggregate structures by the surrounding dispersed polymers. Then, we calculated $\bar{R}_{H,slow}(c)$ again using the zero shear rate viscosity of the solution, η_0, instead of η_s. However, an abnormally small value ($\bar{R}_{H,slow}(c) < 1$ nm) was estimated.

The particle scattering function of the slow-mode component, $P(\theta)_{slow}$, was estimated by the following equation to examine the shape of the aggregate structure in the CC1m solution:

$$P(\theta)_{slow} = \frac{1}{M_{app,slow}}\left(\frac{R_\theta(c)}{Kc}\right)_{slow} \quad (10)$$

Figure 9 shows $P(\theta)_{slow}$ for CC1m solutions plotted versus $R_{g,slow}(c)^2q^2$. Solid curves in Figure 9 represent the theoretical curves for a sphere, a Gaussian chain, and a rod, respectively.[22] For all of the samples examined (0.3∼1.0% (w/w)), $P(\theta)_{slow}$ was plotted between the theoretical curves of the sphere and the Gaussian chain, though the data points for higher angles ($R_{g,slow}(c)^2 \cdot q^2 > 2$) were a little scattered. This indicates that the aggregate structures in the CC1m solution have an intermediate shape between a Gaussian chain and a sphere, that is, like a branched polymer. Single CC1m molecules and the slow-mode components have almost the same R_g (61.3 and 70 nm) but show quite different relaxation times in the semidilute region (Figure 2). The difference in the relaxation times also indicates the difference in the shape of each component.

It is reported in many polymer solutions containing aggregates that the size of the aggregate tends to be larger as the polymer concentration is increased.[5−7] In contrast, the size of aggregates in the CC1m solution is almost independent of the polymer concentration. This will be caused by a mechanism of aggregate characteristic of the mercerized cellulose solutions. However, some factors such as the molecular weight of the polymer will influence the size and the shape of the aggregate. For example, it is reported for poly(*n*-hexyl isocyanate) (PHIC) solutions that the lower the molecular weight of the PHIC sample, the larger the aggregates formed in the solution.[7] Therefore, the comparative study using various samples with different molecular weight or pretreatment of the solution is necessary to examine the characteristics of the aggregate behavior in the mercerized cellulose solution.

Table 1. Diffusion Coefficient, $\bar{D}_T(c)$, Apparent Hydrodynamic Radius, $\bar{R}_H(c)$, and Mean Square Radius of Gyration, $R_g(c)$, of the Fast- and Slow-Mode Component for CC1m Solutions

	fast mode			slow mode		
c/ mg·mL^{-1}	$\bar{D}_{T,fast}(c)$/ 10^{-8}cm^2·s^{-1}	$\bar{R}_{H,fast}(c)$/ nm	$R_{g,app}(c)$/ nm	$\bar{D}_{T,slow}(c)$/ 10^{-10}cm^2·s^{-1}	$\bar{R}_{H,slow}$ (c)/ nm	$R_{g,slow}(c)$/ nm
3.05	2.36	13.8	29.0	7.65	425	75.2
5.04	2.90	11.2	22.8	2.71	1200	78.7
7.04	3.99	8.14	18.5	1.35	2410	70.0
10.0	5.32	6.11	22.2	0.455	7150	59.0

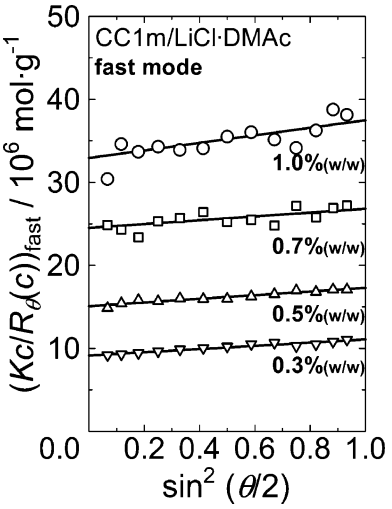

Figure 5. Zimm plot for the fast-mode component of the CC1m solution in 8% (w/w) LiCl·DMAc. $Kc/R_\theta(c)_{fast}$ represents the fast-mode component of $Kc/R_\theta(c)$ for CC1m solutions estimated by eq 5.

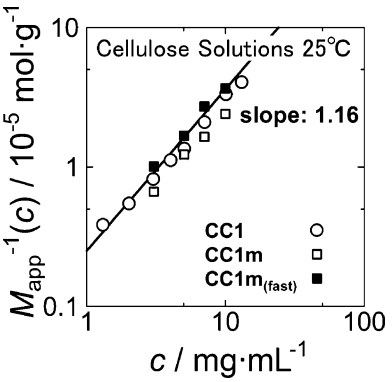

Figure 6. Reciprocal of the apparent molecular mass, $1/M_{app}(c) = (\partial\Pi/\partial c)/RT$, plotted versus the concentration of the polymer, c, for CC1m and CC1 solutions. The values for the fast-mode component of CC1m are also plotted.

Long-Time Relaxation Observed in the Rheological Measurements. The relationship between the long-time relaxation observed in the dynamic viscoelastic measurements for CC1m solutions[13] and the diffusion of the aggregate structure in the solution was investigated. To estimate the relaxation time of the long-time relaxation, τ_L, the relaxation spectra of CC1m solutions, $H_1(\tau)$, were calculated from the storage moduli, $G'(\omega)$, obtained from the dynamic viscoelastic measurements[13] using the first-order approximation equation[20] as follows:

$$H_1(\tau) = \frac{dG'(\tau)}{d \ln \omega}\Big|_{1/\omega=\tau} \quad (11)$$

The derivation of the measured curve was performed by taking the difference because the data points were discrete. Smoothing

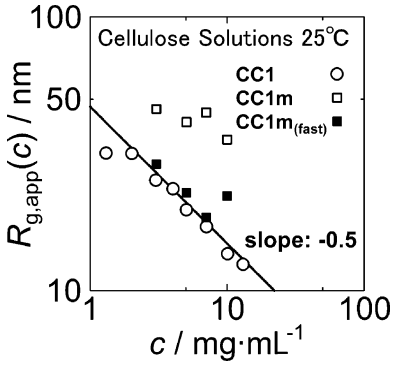

Figure 7. Apparent radius of gyration, $R_{g,app}(c)$, plotted versus the concentration of the polymer, c, for CC1m and CC1 solutions. The values for the fast-mode component of CC1m are also plotted.

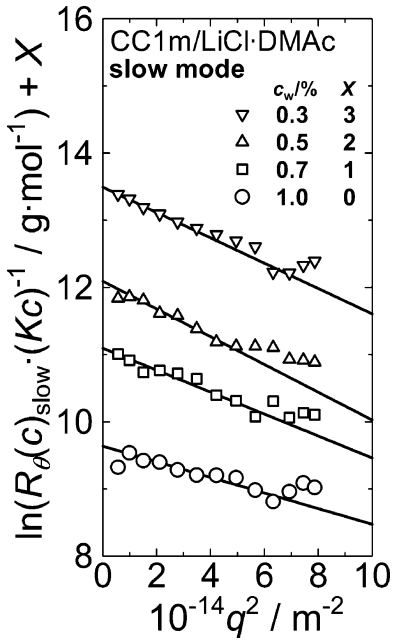

Figure 8. Guinier plot, plotting $\ln(R_\theta(c)/Kc)$ versus q^2, of the slow-mode component of the CC1m solutions. Plots are shifted vertically by a factor, X, to avoid the overlapping of the plots.

of the data points was also performed by averaging the neighboring 2∼5 data points before and after taking the difference to avoid the emphasized noise in the measured curve. Figure 10 shows the relaxation spectra of CC1m solutions calculated by eq 11. The long-time relaxation was observed in the spectrum as a shoulder in the flow region. To determine the position of the shoulder, the first derivative of the curve in Figure 10 was calculated (Figure 11). The shoulder in the spectra was observed as the distinct downward peak in Figure 11 (arrowed in the figure). The relaxation time at the minimum of the downward peak was taken as the relaxation time of the long-time relaxation, τ_L.

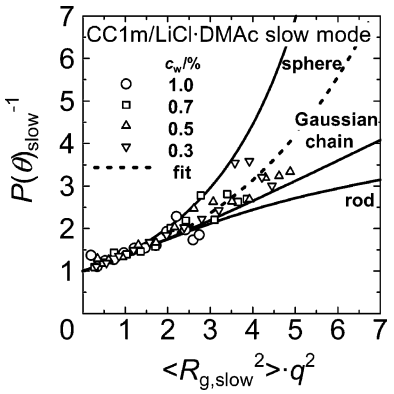

Figure 9. Particle scattering function of the slow-mode component, $P(\theta)_{slow}$, for the CC1m solutions plotted versus $R_{g,slow}(c)^2q^2$. Solid curves represent the theoretical curves for sphere, Gaussian chain, and rod, respectively.[22] The dotted line represents the fitting curve for all of the data points from CC1m solutions.

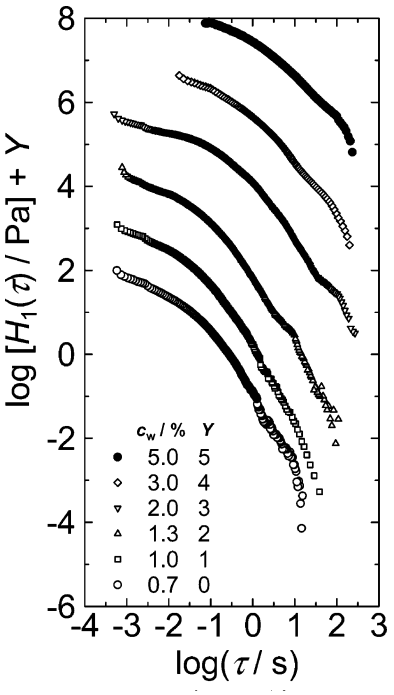

Figure 10. Relaxation spector for CC1m solutions calculated from the storage moduli, $G'(\omega)$,[5] using the first-order approximation equation,[20] eq 11. Plots are shifted vertically by a factor, Y, to avoid the overlapping of the plots.

A characteristic time required for the aggregate structure in the CC1m solution to move the same distance as the diameter by translational diffusion, τ_x, was calculated by the following equation:

$$\sqrt{2\bar{D}_{T,slow}(c)\tau_x} = 2R_{g,slow}(c) \qquad (12)$$

Figure 12 shows the concentration dependence of τ_x and τ_L for CC1m solutions. Both τ_x and τ_L were proportional to c_w^2 and are on an identical straight line in Figure 12. In other words, the two kinds of characteristic times, τ_x, estimated from the SLS and DLS measurements, and τ_L, estimated from the rheological properties, obey an identical concentration dependence. This indicates that the long-time relaxation observed in CC1m solution is the relaxation originating from the translational diffusion of the aggregate structures in the solution.

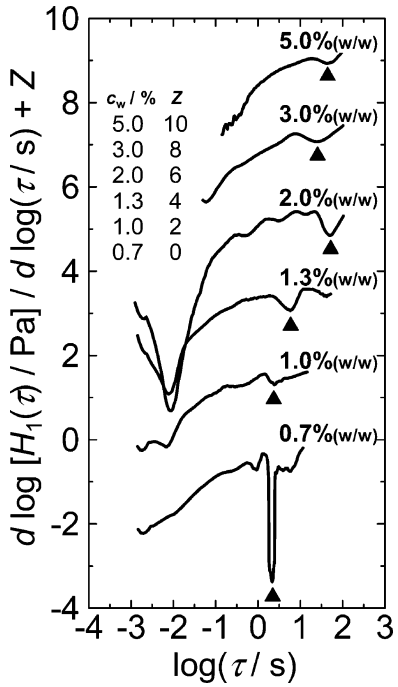

Figure 11. First derivative of the logarithm of relaxation spectra. Plots are shifted vertically by a factor, Z, to avoid the overlapping of the curves.

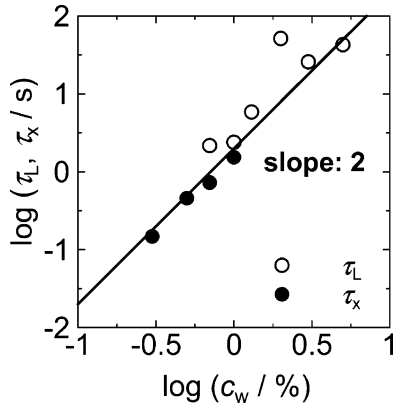

Figure 12. Relaxation time of the long-time relaxation, τ_L, and the characteristic time required for the aggregate structure in the CC1m solution to move the same distance as the diameter by translational diffusion, τ_x, plotted versus the weight concentration of the polymer, c_w.

Conclusion

$R_\theta(c)/Kc$ estimated from the SLS measurements for CC1m semidilute solutions was separated into fast- and slow-mode components by the ratio of the bimodal peak area of G (Γ_i). The values of $M_{app}(c)$ and $R_{g,app}(c)$ for the fast-mode component for CC1m solutions were almost identical with those of the CC1 solution. This indicates that the molecularly dispersed component of CC1m solutions has the same conformation and the same mesh size of polymer entanglements as CC1 solutions. These are consistent with the same concentration dependence of the zero shear rate viscosity and the plateau modulus for CC1m and CC1 solutions estimated by the rheological measurements.[13]

The values of $R_{g,slow}(c)$ estimated from the slow-mode components of CC1m solutions were almost constant ($\approx$70 nm), though the values of $\bar{R}_{H,slow}(c)$ estimated from the DLS measurements increased remarkably with the polymer concentration. This indicates that the size of the aggregate structure in

the CC1m solution does not depend on the polymer concentration, and the accurate size of the aggregate structure in the CC1m solution cannot be estimated only by DLS measurements. The $R_{g,slow}(c)^2q^2$ dependence of $P(\theta)_{slow}$ for CC1m solutions was an intermediate between the theoretical ones of a sphere and a Gaussian chain, indicating that the shape of the aggregate structures in the CC1m solutions has an intermediate shape between a Gaussian chain and a sphere, such as a multiarm polymer. A characteristic time, τ_x, estimated from $\bar{D}_{T,slow}(c)$ and $R_{g,slow}(c)$ showed the same concentration dependence as the relaxation time of the long-time relaxation, τ_L, indicating that the long-time relaxation observed in CC1m solution is the relaxation by the translational diffusion of the aggregate structure in the solutions.

Acknowledgment. This work was supported by a Grant-in-Aid for Scientific Research (B) No. 16380118 from Japan Society for the Promotion of Science.

References and Notes

(1) Guenet, J.-M.; Willmott, N. F. F.; Ellsmore, P. A. *Polym. Commun.* **1983**, *26*, 673.
(2) Koberstein, J. T.; Picot, C.; Benoit, H. *Polymer* **1985**, *26*, 673.
(3) Gan, J. Y.; François, J.; Guenet, J.-M. *Macromolecules* **1986**, *19*, 173.
(4) Heckmeier, M.; Strobl, G. *Macromolecules* **1997**, *30*, 4454.
(5) Ioan, C. E.; Aberle, T.; Burchard, W. *Macromolecules* **2001**, *34*, 326.
(6) Saalwächter, K.; Burchard, W. *Macromolecules* **2001**, *34*, 5587.
(7) Kanao, M.; Matsuda, Y.; Sato, T. *Macromolecules* **2003**, *36*, 2093.
(8) Sedlák, M. *J. Chem. Phys.* **1996**, *105*, 10123.
(9) Matsumoto, T.; Tatsumi, D.; Tamai, N.; Takaki, T. *Cellulose* **2001**, *8*, 275.
(10) Tamai, N.; Aono, H.; Tatsumi, D.; Matsumoto, T. *Nihon Reoroji Gakkaishi (J. Soc. Rheol., Jpn)* **2003**, *31*, 119.
(11) Tamai, N.; Tatsumi, D.; Matsumoto, T. *Biomacromolecules* **2004**, *5*, 422.
(12) Klemm, D.; Philipp, B.; Heinze, T.; Heinze, U.; Wagenknecht, W. *Comprehensive Cellulose Chemistry, vol. 1. Fundamentals and Analytical Methods*; Wiley−VCH: Weinheim, Germany, 1998; Chapter 2.
(13) Aono, H.; Tamai, N.; Tatsumi D.; Matsumoto, T. *Nihon Reoroji Gakkaishi (J. Soc. Rheol., Jpn.)* **2004**, *32*, 169.
(14) Aono, H.; Tatsumi, D.; Matsumoto, T. *J. Polym. Sci. Part: B Polym. Phys.*, submitted.
(15) Turbak, A. F. *Tappi J.* **1984**, *67*, 94.
(16) McCormick, C. L.; Callais, P. A.; Hutchinson, B. H., Jr. *Macromolecules* **1985**, *18*, 2394.
(17) Ishii, D.; Tatsumi, D.; Matsumoto, T. *Biomacromolecules* **2003**, *4*, 1238.
(18) Provencher, S. W. *Comput. Phys. Commun.* **1982**, *27*, 213.
(19) Provencher, S. W. *Comput. Phys. Commun*. **1982**, *27*, 219.
(20) Ferry, J. D. *Viscoelastic Properties of Polymers*, 3rd ed.; John Wiley & Sons: New York, 1980.
(21) de Gennes, P. G. *Scaling Concepts in Polymer Physics*; Cornell University Press: Ithica, NY, 1979.
(22) Kratochvíl, P. *Light scattering from Polymer Solutions*; Huglin, M. B., Ed.; Academic Press: New York, 1972; Chapter 7.

BM050889H